



A wing pod-based millimeter wavelength airborne cloud radar

J. Vivekanandan et al.

A wing pod-based millimeter wavelength airborne cloud radar

J. Vivekanandan, S. Ellis, P. Tsai, E. Loew, W. C. Lee, J. Emmett, M. Dixon, C. Burghart, and S. Rauenbuehler

Earth Observing Laboratory National Center for Atmospheric Research (NCAR), Boulder, CO, USA

Received: 23 January 2015 – Accepted: 10 March 2015 – Published: 14 April 2015

Correspondence to: J. Vivekanandan (vivek@ucar.edu)

Published by Copernicus Publications on behalf of the European Geosciences Union.

[Title Page](#)

[Abstract](#)

[Introduction](#)

[Conclusions](#)

[References](#)

[Tables](#)

[Figures](#)



[Back](#)

[Close](#)

[Full Screen / Esc](#)

[Printer-friendly Version](#)

[Interactive Discussion](#)



Abstract

This paper describes a novel, airborne pod-based millimeter wavelength radar. Its frequency of operation is 94 GHz (3 mm wavelength). The radar has been designed to fly on the NCAR Gulfstream V HIAPER aircraft; however, it could be deployed on other similarly equipped aircraft. The pod-based configuration occupies minimum cabin space and maximizes scan coverage. The radar system is capable of collecting observations in a staring mode between zenith and nadir or in a scanning mode. Standard pulse-pair estimates of moments and raw time series of backscattered signals are recorded. The radar system design and characteristics, as well as techniques for calibrating reflectivity and correcting Doppler velocity for aircraft attitude and motion are described. The radar can alternatively be deployed in a ground-based configuration, housed in the 20 ft shipping container it shares with the High Spectral Resolution Lidar (HSRL). The radar was tested both on the ground and in flight. Preliminary measurements of Doppler and polarization measurements were collected and examples are presented.

1 Introduction

One attractive feature of millimeter (mm) wavelength radar systems is their ability to detect micron-sized particles that constitute liquid and ice clouds. Even though the upper limit of transmit power at millimeter wavelength band is more than 25 dB lower than at centimeter bands (S, C and X-bands), the larger backscatter cross section of particle sizes smaller than the wavelength (Rayleigh scattering) significantly improves the detection limit (Lhermitte, 1987, Clothiaux et al., 1995). The radar cross section at W-band is 40 dB larger than at X-band in the Rayleigh scattering regime. Another advantage of mm wavelength radars for airborne deployments is that the radar antenna is much smaller in size than the cm wavelength antenna for a specified angular beam resolution and the overall radar size is more compact. Therefore it is easier to achieve

GID

5, 117–159, 2015

A wing pod-based millimeter wavelength airborne cloud radar

J. Vivekanandan et al.

Title Page

Abstract

Introduction

Conclusions

References

Tables

Figures

⏪

⏩

◀

▶

Back

Close

Full Screen / Esc

Printer-friendly Version

Interactive Discussion



A wing pod-based millimeter wavelength airborne cloud radar

J. Vivekanandan et al.

[Title Page](#)

[Abstract](#)

[Introduction](#)

[Conclusions](#)

[References](#)

[Tables](#)

[Figures](#)

[⏪](#)

[⏩](#)

[◀](#)

[▶](#)

[Back](#)

[Close](#)

[Full Screen / Esc](#)

[Printer-friendly Version](#)

[Interactive Discussion](#)



finer beam resolution $< 1^\circ$ and range resolution on the order of tens of meters. Lower sidelobes and larger signal-to-clutter ratio at mm wavelength band radars significantly enhance their detection capability, in particular close to the radar (Kropfli and Kelly, 1996). However, mm wavelength radar signals are more susceptible to attenuation. The amount of attenuation is proportional to the intensity of the precipitation and gaseous absorption (Ellis and Vivekanandan, 2010, 2011). As a result, they are not suitable for observing even moderate precipitation.

Due to the above described advantages of compact size, higher spatial resolution, and enhanced sensitivity, scanning or vertically-pointing ground-based mm wavelength radars are used to study stratocumulus (Vali et al., 1998; Kollias and Albrecht 2000), fair-weather cumulus (Kollias et al., 2000, 2001, 2002, 2007) and fog properties (Hamazu et al., 2003). Airborne mm wavelength radars have been used for atmospheric remote sensing since the early 1990s (Pazmany et al., 1994; Horie et al., 2000; Hanesiak et al., 2010; Wolde and Vali, 2001a, b). Airborne cloud radar systems such as the University of Wyoming King Air Cloud Radar (WCR) and the NASA ER-2 Cloud Resolving System (CRS) can observe clouds in remote regions and over the oceans (Li et al., 2004, WCR, 2012).

The scientific requirements of mm wavelength radar are mainly driven by climate and cloud process studies. Millimeter wavelength radar with dual-Doppler and dual-Polarization capability is highly desirable for the concurrent estimation of dynamical and microphysical properties of clouds and precipitation. A polarization Doppler radar with dual-wavelength and dual-beams is capable of retrieving microphysical properties and two-dimensional winds.

In 2005, a survey of the cloud radar user community was conducted in order to assess needs and help guide the design of a mm wavelength radar on the National Science Foundation (NSF) Gulfstream V (GV), High-Performance Instrumented Airborne Platform for Environmental Research (HIAPER) aircraft (Laursen et al., 2006), named HIAPER Cloud Radar (HCR). Results of the survey indicated a common preference for narrow beam W-band radar with polarimetric and single Doppler capabilities with

A wing pod-based millimeter wavelength airborne cloud radar

J. Vivekanandan et al.

[Title Page](#)

[Abstract](#)

[Introduction](#)

[Conclusions](#)

[References](#)

[Tables](#)

[Figures](#)

[⏪](#)

[⏩](#)

[◀](#)

[▶](#)

[Back](#)

[Close](#)

[Full Screen / Esc](#)

[Printer-friendly Version](#)

[Interactive Discussion](#)



tating reflector, a 12 inch lens antenna and a pressure vessel. The pod is not environmentally controlled. In order to ensure a stable radar operation under conditions of temperature and pressure from sea level to 45 000 ft m.s.l., all radar electronics including the high voltage transmitter are housed in the pressure vessel. This pressure vessel is 60'' in length and 15'' in diameter and pressurized with dry nitrogen. To further mitigate potential arcing in the externally located waveguide and antenna feed, the antenna and associated waveguide are also pressurized through the pressure vessel. The 12 inch lens antenna illuminates a rotatable reflector plate that allows the coverage of a 220° sector including zenith and nadir directions in the plane normal to the fuselage.

3 Radar system description

This section provides brief descriptions of the various radar sub-systems of the HCR including the transmitter and transceiver, antenna and radome, and the data system.

3.1 Transmitter and transceiver

A block diagram of the radar transceiver is shown in Fig. 3. The HCR uses a conduction-cooled extended interaction klystron amplifier (EIKA) to amplify the signal for transmission. The EIKA is similar to the one used in the CloudSat radar (Stephens et al., 2002). The EIKA, its modulator and the entire receiver electronics are housed in the pressure vessel. Since the modulator is rated for a maximum operating altitude 7000 ft m.s.l., the pressure vessel must be maintained between 15 and 16 PSIA by a supplemental pressurization system. Both the EIKA and modulator are designed to operate at a 5 % duty cycle.

The HCR system transmits a single frequency pulse with a programmable pulse width that can range from 256 to 1024 ns (38.4 to 153.6 m range resolution) at a 10 kHz PRF. A dual-channel receiver is used for measuring co- and cross-polarization signals.

A wing pod-based millimeter wavelength airborne cloud radar

J. Vivekanandan et al.

[Title Page](#)

[Abstract](#)

[Introduction](#)

[Conclusions](#)

[References](#)

[Tables](#)

[Figures](#)

[⏪](#)

[⏩](#)

[◀](#)

[▶](#)

[Back](#)

[Close](#)

[Full Screen / Esc](#)

[Printer-friendly Version](#)

[Interactive Discussion](#)



The motors are programmed to rotate from -10° from Zenith (toward the fuselage) to 210° (30° from nadir) perpendicular to along track direction and from -6 to $+6^\circ$ in the tilt axis. The tilt axis adjustment compensates for the aircraft pitch. Both rotation and tilt are controlled in real-time to compensate for platform motion to minimize the bias of aircraft motion into the velocities. A CMIGITS-III inertial reference unit mounted in the nose cone, just 12 inches forward of the reflector, provides the necessary spatial reference and minimizes the moment arm. A consequence of using a reflector plate is that the polarization of the transmitted waveform changes as the reflector plate rotates. A rotational transformation will be used to recover intrinsic polarization state of the received signal (Vivekanandan et al., 1990).

3.3 Data system

HCR places some unique requirements on data system characteristics such as size, weight and environmental factors. Radar control, preliminary signal processing and data display and archiving are handled by a computer located on a 19 inch rack mounted in the aircraft cabin, while radar timing, real-time data acquisition and house-keeping are handled by a data system located in the pod. Housekeeping structure consists of system status, GPS time, antenna angle, and aircraft attitude. The cabin and pod data systems are linked by a fiber optic, gigabit network connection. These connections relay radar control commands from the cabin as well as digital time series data, housekeeping and status from the pod.

The received signal is digitized at the rate of 125 MHz. Both in-phase and quadrature data are archived in HCR. Standard moment products such as reflectivity, Doppler velocity and spectrum width are provided in CfRadial format (www.eol.ucar.edu/content/standard-data-formats). The moment products are processed and displayed in real-time on the archiving computer in the cabin. Data rates for the phase A system are $\sim 70 \text{ Mbytes s}^{-1}$. This is handled by a single gigabit Ethernet connection coupled to a 24 Terabyte redundant array of disks (RAID). Data are simultaneously written to the

RAID and two removable external USB3 drives. The USB3 drives offer quick access to data after completion of the research flight.

All HCR data are archived on the NCAR High Performance Storage System (HPSS), a state-of-the-art Data Center storage facility. Data are available in a CfRadial format and EOL provides basic tools to access those data. EOL supports basic software for display of radar data, editing of radar fields, and derivation of several value-added products.

4 Performance characteristics of the HCR

An overview of the performance characteristics achieved by the design of HCR described in Sect. 3 is presented here. For ease of reference some of the important system parameters and performance characteristics under typical operations for HCR are listed in Table 1.

4.1 Measurement accuracy of mean velocity and reflectivity

The measurement accuracy of Doppler radial velocity and reflectivity are a function of time-to-independence (T_D), PRF, and signal-to-noise ratio (SNR) (Doviak and Zrnic, 1993). Time-to-independence determines the interval between two radar measurements that are statistically independent. It is a function of transmit frequency and spectrum width (Bringi and Chandrasekar, 2001). In the case of W-band, T_D is smaller than the corresponding value of cm wavelength radars. As a result, more independent samples are collected at W-band for a specified dwell time and Doppler spectrum width as compared to larger wavelengths such as S, C, and X-bands.

Figure 5 shows the number of independent samples required as a function of signal-to-noise ratio (SNR) for various accuracy values of measured mean radial velocity at W-band. For 10 independent samples, an SNR of 3.5 dB is required for estimating radial velocity within 0.2 m s^{-1} accuracy. Since T_D at W-band is smaller than at cm-band, more

GID

5, 117–159, 2015

A wing pod-based millimeter wavelength airborne cloud radar

J. Vivekanandan et al.

[Title Page](#)

[Abstract](#)

[Introduction](#)

[Conclusions](#)

[References](#)

[Tables](#)

[Figures](#)

[⏪](#)

[⏩](#)

[◀](#)

[▶](#)

[Back](#)

[Close](#)

[Full Screen / Esc](#)

[Printer-friendly Version](#)

[Interactive Discussion](#)



accurate estimates of mean velocity can be achieved in a shorter dwell time interval. Therefore, the HCR offers finer spatial resolution and more accurate radial velocity than a cm-wavelength band airborne radar.

The standard error in HCR reflectivity as a function of Doppler spectrum width and number of samples is shown in Fig. 6 (Bringi and Chandrasekar, 2001). Since the number of independent samples increase as spectrum width increases, standard error reduces for a specified number of samples at higher spectral widths. As PRF of HCR is 10 kHz, averaging 1000 samples or 0.1 s time-average reduces the standard error of reflectivity to less than 0.5 dB.

4.2 Sensitivity and spatial resolution

For the technical specifications listed in Table 1, Fig. 7 shows the sensitivity of the HCR as a function of range for a single pulse-pair measurement. The curves shown in the figure take into account radome attenuation, and receiver filter loss. The sensitivity of the HCR can be enhanced by increasing the transmit pulse width and by performing noise subtraction and temporal averaging of the received sample power. Since the transmit pulse width can be varied between 0.256 and 1.024 μ s, the sensitivity of the radar can be enhanced by a transmitting longer pulse at the expense of range resolution. For example, a factor of two coarser in range resolution improves sensitivity by 6 dB as shown in Fig. 7. Averaging over 0.1 s and noise subtraction improves the minimum reflectivity by 8 dB. In summary, HCR sensitivity is -41.4 dBZ at 1 km for a 0.5 μ s transmit pulse width when the received signal is corrected for noise and are averaged over 0.1 s.

Pulse-pair estimates are averaged over a time interval to reduce fluctuations in the Doppler moment estimates, namely, reflectivity, mean velocity and spectrum width. Figure 8 shows the total number of samples verses along track resolution for a specified aircraft speed and PRF. For 0.1 s or 1000 sample averaging, along track resolution is 20 m.

A wing pod-based millimeter wavelength airborne cloud radar

J. Vivekanandan et al.

[Title Page](#)

[Abstract](#)

[Introduction](#)

[Conclusions](#)

[References](#)

[Tables](#)

[Figures](#)



[Back](#)

[Close](#)

[Full Screen / Esc](#)

[Printer-friendly Version](#)

[Interactive Discussion](#)



Since the PRF is 10 kHz, around 100 statistically independent samples can be obtained from clouds with Doppler spectrum width $> 0.4 \text{ ms}^{-1}$. It should be noted, the number of independent samples is determined by the dwell time of the beam, which is primarily determined by aircraft speed and Doppler spectrum width of the cloud.

5 Data quality assurance

5.1 Radar system calibration

Obtaining an accurate system calibration is essential for HCR's scientific missions. Calibration schemes are broadly divided into two categories: internal calibration and external calibration. Internal calibration methods include measurements using a noise source, calibrated test signal source. External calibration methods include measurements of a corner reflector cross section, backscatter measurements from light precipitation and reflection from the ocean surface.

5.1.1 Internal calibration

Figure 3 shows two internal calibration paths of HCR. The transmit signal is coupled from its path and monitored on a pulse by pulse basis by a W-band detector (path colored blue). A known noise source is injected into the receiver path to monitor receiver gain (path colored red). The noise source is switched on to track differential changes in the receiver gain during operation as the receiver gain fluctuates with ambient temperature. The advantage of noise source is its stable performance of better than 0.004 dB as the ambient temperature varies over 30° . The stable noise source reference allows robust monitoring of the receiver calibration. Due to the limited space in the pressure vessel, the noise source calibration method is configured only for the vertical polarimetric channel. The gain of the horizontal polarimetric channel can be estimated from the physical temperature of the low noise amplifier in conjunction with the known gain of the calibrated vertical polarimetric channel.

A wing pod-based millimeter wavelength airborne cloud radar

J. Vivekanandan et al.

[Title Page](#)

[Abstract](#)

[Introduction](#)

[Conclusions](#)

[References](#)

[Tables](#)

[Figures](#)

[⏪](#)

[⏩](#)

[◀](#)

[▶](#)

[Back](#)

[Close](#)

[Full Screen / Esc](#)

[Printer-friendly Version](#)

[Interactive Discussion](#)



5.1.2 External calibration using measurements from light rain

Since the reflectivity remains similar for a wide range of rain rates, observations from light rain can be used for verifying the W-band reflectivity (Hogan et al., 2003). At W-band, attenuation and Mie scattering dominate scattering from particle sizes > 0.3 mm.

The combination of Mie scattering and attenuation effects causes W-band reflectivity measurements at near ranges to saturate (Hogan et al., 2003). Electromagnetic scattering and wave propagation models can be used for quantifying reflectivities of light rain (Vivekanandan et al., 1991). The computation of reflectivity requires the specification of raindrop size distribution parameters. Raindrop size distribution parameters are varied over their natural variations (Ulbrich, 1983). Figure 9a–c shows histograms of computed rain rate, median volume diameters and number concentration parameters for rain rates between 5 and 20 mm h⁻¹. For these parameters of raindrop size distributions, reflectivity values were calculated using scattering amplitudes (Vivekanandan et al., 1991). Particle shapes were assumed spherical since differential reflectivity for rain at W-band is less than 0.5 dB. The modeled reflectivity values at 200 m distance from the radar are shown in Fig. 9d. The mean value of the modeled reflectivity is 19.0 dBZ and SD is 0.5 dB.

Figure 10a–c shows ground-based HCR reflectivity, radial velocity and linear depolarization measurements in rain rates between 5 and 10 mm h⁻¹ for fixed beam pointing as a function of time. The measurements were taken on 8 September 2014 around 21:40 UTC. The radar beam was fixed at 30 elevation from horizontal. The reflectivity structure shows frozen precipitation at the top layer, aggregation in the mid-layer and light rain below 400 m a.g.l. Increased radial velocity and a strong gradient in LDR structure shows the melting level is around 0.5 km a.g.l. A canopy was used for keeping the radome dry during the rain event. A wet radome attenuates radar signals and will introduce a large uncertainty in reflectivity measurements (Hogan et al., 2003).

A histogram of reflectivity at 250 m range is shown in Fig. 10d. The mean value of measured reflectivity is 17.5 dB. This value is 1.5 dB lower than the expected value

A wing pod-based millimeter wavelength airborne cloud radar

J. Vivekanandan et al.

[Title Page](#)[Abstract](#)[Introduction](#)[Conclusions](#)[References](#)[Tables](#)[Figures](#)[Back](#)[Close](#)[Full Screen / Esc](#)[Printer-friendly Version](#)[Interactive Discussion](#)

eraged to the more practical 10 Hz nominal time resolution, or any other user-specified temporal resolution. Since HCR nominally runs with a pulse repetition frequency of 10 000 Hz there are 100 samples to compute the moments at 100 Hz, which is sufficient for platform motion correction. This strategy reduces the radial errors in SW and V_r that occur if the platform accelerates at a time scale shorter than the resolution of the navigation data.

6 Measurement examples

The radar is capable of estimating winds and microphysics to a range of 15 km range with 19.2 m gate spacing. The HCR can be operated in scanning and staring modes for detecting cloud boundaries, cloud liquid and ice and also for estimating radial winds. Along track resolution is nominally about 60 m. There is a real-time, on-board display of the HCR measurements. Its capability to serve as a surveillance radar is very limited, as attenuation, and Mie scattering at the W-band frequency would limit maximum detectable reflectivity to about 30 dBZ. The dynamic range of HCR reflectivity is between -40 and 30 dBZ. Reflectivity can be estimated within ± 0.5 dB accuracy. In weakly and non-precipitating conditions, ice and liquid water content amounts can be estimated from reflectivity measurements.

The HCR will participate in its first field deployment in the summer of 2015. The project is named CSET (Cloud System Evolution in the Trades) and aims to study the characteristics and evolution of stratocumulus clouds over the eastern Pacific Ocean. In preparation for the inaugural HCR project, data have been collected during two test flight campaigns as well as in the ground-based configuration. The motivation for the data collection was primarily engineering tests of calibration, reliability, and platform motion correction. Also, being developed are real-time displays onboard the aircraft and analysis tools for post-processing display of the HCR moment and Doppler spectral data. During research flights the HCR operator will be able to monitor system performance and real-time data display. Summary images will be automatically generated

A wing pod-based millimeter wavelength airborne cloud radar

J. Vivekanandan et al.

[Title Page](#)

[Abstract](#)

[Introduction](#)

[Conclusions](#)

[References](#)

[Tables](#)

[Figures](#)



[Back](#)

[Close](#)

[Full Screen / Esc](#)

[Printer-friendly Version](#)

[Interactive Discussion](#)



at user-specified time intervals and can be sent to a land-based operations center via the GV communications system. Therefore scientists on the ground and in the aircraft can coordinate (via internet chat) during the mission.

Even though there was no particular phenomenon being studied during HCR testing, several interesting data sets have been collected in different weather conditions. These data illustrate the capability and measurement potential of the HCR. Examples of these data sets are shown in this section.

6.1 Airborne data

6.1.1 Winter precipitation with convective features

Figure 12 shows B-scan plots of Z_e , and V_r (corrected for platform motion) collected by HCR on the GV looking nadir on 23 February 2013 at 02:11 UTC during an upslope snow event along the Front Range of Colorado. Shown is one minute of data and the vertical axis indicates altitude above mean sea level (m.s.l.) and the horizontal axis shows the horizontal distance the GV flew during the minute. The ground echo can be seen as the high reflectivity (black) with $0 \text{ ms}^{-1} V_r$ at about the 1.7 km m.s.l. As per the standard convention receding wind from radar has positive sign and approaching wind toward radar has negative sign. The 00:00 UTC Denver sounding from the National Weather Service (not shown) indicated the surface temperature was only slightly above 0°C and decreased rapidly with height to about -35°C at 7 km m.s.l. Two distinct cloud layers were detected by HCR at this time. Small scale ($< 1 \text{ km}$) convective features are seen at the top of the echo layer between roughly 6 and 7 km m.s.l. The wind at this level was Northwesterly at about 25 kts according to the sounding and the plane was flying towards the Southwest. The base of the cloud undulates up and down along the horizontal at a scale that is larger than the convective features on top. This layer shows distinct regions of receding, or downward, (positive V_r) and approaching, or upward, (negative V_r) velocity measurements. The largest positive V_r is over 1 ms^{-1} and the largest negative V_r is about 0.8 ms^{-1} . The measured V_r is a combination of the fallspeed

A wing pod-based millimeter wavelength airborne cloud radar

J. Vivekanandan et al.

[Title Page](#)

[Abstract](#)

[Introduction](#)

[Conclusions](#)

[References](#)

[Tables](#)

[Figures](#)

[⏪](#)

[⏩](#)

[◀](#)

[▶](#)

[Back](#)

[Close](#)

[Full Screen / Esc](#)

[Printer-friendly Version](#)

[Interactive Discussion](#)



of the particles and the air motion, so the upward V_r measurements indicate vertical air motion and the pattern of alternating up and downward motion is indicative of waves. The lower layer shown in Fig. 13 is observed to be about 2 km thick and is a result of Easterly upslope flow evident on the Denver sounding. Many fine-scale features are seen in the Ze and V_r fields in the lower level.

6.1.2 Stratiform rain and drizzle

Figure 13 shows B-scan displays of Ze, V_r (platform motion corrected), and also corrected SW. The data were collected by HCR pointing nadir from the GV on 11 October 2013 at 19:26 UTC. Again one minute of data is shown and the horizontal axis designates the distance the aircraft travelled in that time. The weather is a stratiform rain and drizzle case. The echo in the low levels is about 3 km thick. The melting layer is apparent at just below 2 km m.s.l. and is indicated by an increase in the Ze, V_r and SW. The increase in Ze is due to the increase in the refractive index of liquid over snow and ice crystals. As the ice melts the density increases and thus so does the fallspeed, resulting in the increase of V_r . The increase of SW below the melting layer is due, at least partially, to the fact that liquid drops exhibit a larger range of fall speeds and larger differences in terminal fallspeed for different sizes. Additional turbulence in the boundary layer will also contribute to the increase in measured SW. There is also a small cirrus cloud at about 9 km m.s.l. detected with measured Ze values between about -30 and -39 dBZ. Interestingly the measured V_r varies in the cirrus from roughly 0 to almost 1 ms^{-1} .

6.2 Ground-based data

The HCR was also deployed in its ground-based configuration with coincident high spectral resolution lidar (HSRL) (Eloranta, 2005) data looking vertically in November of 2013 in Boulder Colorado. Figure 15 shows B-scan displays of HCR Ze and V_r on 22 November 2013 from 04:00 to 05:00 UTC during a snow event. Light snow was

A wing pod-based millimeter wavelength airborne cloud radar

J. Vivekanandan et al.

[Title Page](#)

[Abstract](#)

[Introduction](#)

[Conclusions](#)

[References](#)

[Tables](#)

[Figures](#)

[⏪](#)

[⏩](#)

[◀](#)

[▶](#)

[Back](#)

[Close](#)

[Full Screen / Esc](#)

[Printer-friendly Version](#)

[Interactive Discussion](#)



Discussion Paper | Discussion Paper | Discussion Paper | Discussion Paper | Discussion Paper

requirements for desired accuracy in radar measurements can be used for designing an optimal data collection strategy for a specified scientific mission.

The current system is a single frequency, polarimetric Doppler radar. The transmit and receive systems are designed to accommodate implementation of pulse compression to achieve finer range resolution. The layout of the pod will accommodate a second radar at K_a -band for dual-wavelength measurements. Inclusion of dual-wavelength capability will significantly enhance the accuracies of retrieved cloud microphysical quantities.

Internal and external calibration schemes are used for monitoring data quality. For radar systems, internal calibration is important to track changes in the receiver gains. The methodology presented in this paper for calibrating reflectivity makes use of light rain as a calibration target and it assures standard error reflectivity measurements < 0.5 dB. The amount of aircraft motion contribution to airborne Doppler measurements is determined by aircraft velocity along the radar beam pointing direction. This requires precise estimates of the antenna pointing angle and aircraft attitude and velocity. The two-step procedure for correcting the influence of platform motion on measured radial velocity assures better than 0.1 ms^{-1} .

Preliminary measurements show the radar is capable of estimating accurate reflectivity and velocity observations for climate science and cloud process studies that are dominated by cloud liquid and cloud ice particles. The HCR will serve the atmospheric science research community by adding mm wavelength remote sensing capabilities to the HIAPER aircraft. The HCR measurements in conjunction with other HIAPER instrumentation have the potential to significantly increase our understanding of cloud physics.

Acknowledgements. NCAR is primarily funded by the National Science Foundation. This material is based upon work supported by the National Science Foundation under cooperative Grant Number NSF0015 and MO904 552. Any opinions, findings, and conclusions or recommendations expressed in this material are those of the author(s) and do not necessarily reflect the views of the National Science Foundation.

GID

5, 117–159, 2015

A wing pod-based millimeter wavelength airborne cloud radar

J. Vivekanandan et al.

[Title Page](#)

[Abstract](#)

[Introduction](#)

[Conclusions](#)

[References](#)

[Tables](#)

[Figures](#)

[⏪](#)

[⏩](#)

[◀](#)

[▶](#)

[Back](#)

[Close](#)

[Full Screen / Esc](#)

[Printer-friendly Version](#)

[Interactive Discussion](#)



The guidance and support of Al Cooper of NCAR was invaluable throughout the development. The authors would like to thank Mike Strong for his technical expertise and leadership in the project. We also thank James Ranson, David Allen and Karl Schwenz of the NCAR Design and Fabrication Services for fabrication and design of mechanical infrastructure. The authors also thank Sam Haimov of the University of Wyoming for many helpful technical discussions. The authors appreciate Charlie Martin's extensive software development for the initial prototype. The authors appreciate the thoughtful and helpful manuscript review by John Hubbert of NCAR.

References

- Bringi, V. N. and Chandrasekar, V.: Polarimetric Doppler Weather Radar, Cambridge University Press, New York, 2001.
- Bosart, B. L., Lee, W. C., and Wakimoto, R. M.: Procedures to improve the accuracy of airborne Doppler radar data, *J. Atmos. Ocean. Tech.*, 19, 322–339, 2002.
- Brown, P. R., Illingworth, A. J., Heymsfield, A. J., McFarquhar, G. M., Browning, K. A., and Gosset, M.: The role of spaceborne millimeter-wave radar in the global monitoring of ice clouds, *J. Appl. Meteorol.*, 34, 2346–2366, 1995.
- Clothiaux, E. E., Miller, M. A., Albrecht, B. A., Ackerman, T. P., Verlinde, J., Babb, D. M., Peters, R. M., and Syrett, W. J.: An evaluation of a 94-GHz radar for remote sensing of cloud properties, *J. Atmos. Ocean. Tech.*, 12, 201–229, 1995.
- Danne, O., Quante, M., Milferstädt, D., Lemke, H., and Raschke, E.: Relationships between Doppler spectral moments within large-scale cirro- and altostratus cloud fields observed by a ground-based 95-GHz cloud radar, *J. Appl. Meteorol.*, 38, 175–189, doi:10.1175/1520-0450(1999)038<0175:RBDSMW>2.0.CO;2, 1999.
- Donovan, D. P. and van Lammeren, A. C. A. P.: Cloud effective particle size and water content profile retrievals using combined lidar and radar observations 1, theory and examples, *J. Geophys. Res.*, 106, 27425–27448, 2001.
- Doviak, R. J. and Zrnic, D.: Doppler Radar and Weather Observations, Academic Press, San Diego, CA, 562 pp., 1993.

A wing pod-based millimeter wavelength airborne cloud radar

J. Vivekanandan et al.

[Title Page](#)

[Abstract](#)

[Introduction](#)

[Conclusions](#)

[References](#)

[Tables](#)

[Figures](#)

[⏪](#)

[⏩](#)

[◀](#)

[▶](#)

[Back](#)

[Close](#)

[Full Screen / Esc](#)

[Printer-friendly Version](#)

[Interactive Discussion](#)



A wing pod-based millimeter wavelength airborne cloud radar

J. Vivekanandan et al.

[Title Page](#)

[Abstract](#)

[Introduction](#)

[Conclusions](#)

[References](#)

[Tables](#)

[Figures](#)

[⏪](#)

[⏩](#)

[◀](#)

[▶](#)

[Back](#)

[Close](#)

[Full Screen / Esc](#)

[Printer-friendly Version](#)

[Interactive Discussion](#)



Ulaby, R. T., Moore, R. K., and Fung, A. K.: Microwave Remote Sensing Active and Passive, Vol. II: Radar Remote Sensing and Surface Scattering and Emission Theory, Artech House, Inc., Norwood, Massachusetts, 1982.

Ulbrich, C. W.: Natural variations in the analytical form of the raindrop size distribution, *J. Clim. Appl. Meteorol.*, 22, 1764–1775, 1983.

Vali, G., Kelly, R. D., French, J., Haimov, S., Leon, D., McIntosh, R. E., and Pazmany, A.: Finescale structure and microphysics of coastal stratus, *J. Atmos. Sci.*, 55, 3540–3564, 1998.

Vivekanandan, J., Turk, J., Stephens, G. L., and Bringi, V. N.: Microwave radiative transfer studies using combined multiparameter radar and radiometer measurements during COHMEX, *J. Appl. Meteorol.*, 29, 561–585, 1990.

Vivekanandan, J., Adams, W. M., and Bringi, V. N.: Rigorous approach to polarimetric radar modeling of hydrometeor orientation distributions, *J. Appl. Meteorol.*, 30, 1053–1063, 1991.

Wang, Z., French, J., Vali, G., Wechsler, P., Haimo, S., Rodi, A., Deng, M., Leon, D., Snider, J., Peng, L., and Pazmany, A.: Single aircraft integration of remote sensing and in situ sampling for the study of cloud microphysics and dynamics, *B. Am. Meteorol. Soc.*, 93, 653–668, 2012.

Wolde, M. and Vali, G.: Polarimetric signatures from ice crystals observed at 95 GHz in winter clouds, part I: dependence on crystal form, *J. Atmos. Sci.*, 58, 828–841, 2001a.

Wolde, M. and Vali, G.: Polarimetric signatures from ice crystals observed at 95 GHz in winter clouds. Part II: Frequency of occurrence, *J. Atmos. Sci.*, 58, 842–849, 2001b.

WCR: Wyoming cloud radar, University of Wyoming, Laramie, available at: <http://www-das.uwyo.edu/wcr/> (last access: 5 April 2015), 2012.

A wing pod-based millimeter wavelength airborne cloud radar

J. Vivekanandan et al.

[Title Page](#)

[Abstract](#)

[Introduction](#)

[Conclusions](#)

[References](#)

[Tables](#)

[Figures](#)

[⏪](#)

[⏩](#)

[◀](#)

[▶](#)

[Back](#)

[Close](#)

[Full Screen / Esc](#)

[Printer-friendly Version](#)

[Interactive Discussion](#)



Table 1. HCR Specifications.

Parameter	Specification
Transmit frequency	94.4 GHz, W-band
Antenna diameter	0.30 m, Lens antenna
Antenna gain	46.21 dB
Beamwidth	0.68°
Peak power	1.6 kW
Pulse width	0.256–1.024 μ s
PRF	10 kHz
System noise power	–104 dBm
Noise figure	9.4 dB
First and Second IF	156.25 and 1406.25 MHz
Sensitivity (0 dB SNR, single pulse pair)	–33.6 dBZ at 1 km
Sensitivity (–6.5 dB SNR, 0.1 s averaging)	–41.4 dBZ at 1 km
Minimum linear depolarization ratio	–29 dB
Unambiguous Velocity	$\pm 7.75 \text{ ms}^{-1}$
Along track resolution and dwell time	20 m, and 100 ms

Table A1. List of Acronyms.

CRS	Cloud Radar System
CfRadial	Climate and forecasting radial
dBZ	Radar reflectivity factor
EIKA	Extended interaction klystron amplifier
EOL	Earth Observing Laboratory
FAA	Federal aviation Administration
GV	Gulfstream V
HCR	HIAPER Cloud Radar
HALO	High-altitude long-range research aircraft
HPSS	High Performance Storage System
HIAPER	High-Performance Instrumented Airborne Platform for Environmental Research
HSRL	High Spectral Resolution Lidar
ICPR	Integrated cross-polar ratio
IF	Intermediate frequency
LNA	Low noise amplifier
LDR	Linear depolarization ratio
m.s.l.	Mean sea level
NCAR	National Center for Atmospheric Research
NOAA	National Oceanic and Atmospheric Administration
NSF	National Science Foundation
PRF	Pulse repetition frequency
QC	Quality control
RAID	Redundant array of inexpensive disks
RF	Radio frequency
RHI	Range height indicator
Rx	Receiver
SNR	Signal-to-noise ratio
Solo	Software for radar translation, visualization, editing and interpolation
STSR	Simultaneously transmit and simultaneously receive
T_D	Time-to-independence
Tx	Transmitter
V	Vertical
V_r	Radial velocity
Ze	Reflectivity
λ_o	The transmit wavelength

A wing pod-based millimeter wavelength airborne cloud radar

J. Vivekanandan et al.

[Title Page](#)

[Abstract](#)

[Introduction](#)

[Conclusions](#)

[References](#)

[Tables](#)

[Figures](#)



[Back](#)

[Close](#)

[Full Screen / Esc](#)

[Printer-friendly Version](#)

[Interactive Discussion](#)





Figure 1. View of NCAR pod mounted below surface of right wing.

GID

5, 117–159, 2015

A wing pod-based millimeter wavelength airborne cloud radar

J. Vivekanandan et al.

[Title Page](#)

[Abstract](#)

[Introduction](#)

[Conclusions](#)

[References](#)

[Tables](#)

[Figures](#)

[⏪](#)

[⏩](#)

[◀](#)

[▶](#)

[Back](#)

[Close](#)

[Full Screen / Esc](#)

[Printer-friendly Version](#)

[Interactive Discussion](#)



A wing pod-based millimeter wavelength airborne cloud radar

J. Vivekanandan et al.

[Title Page](#)

[Abstract](#)

[Introduction](#)

[Conclusions](#)

[References](#)

[Tables](#)

[Figures](#)

[⏪](#)

[⏩](#)

[◀](#)

[▶](#)

[Back](#)

[Close](#)

[Full Screen / Esc](#)

[Printer-friendly Version](#)

[Interactive Discussion](#)

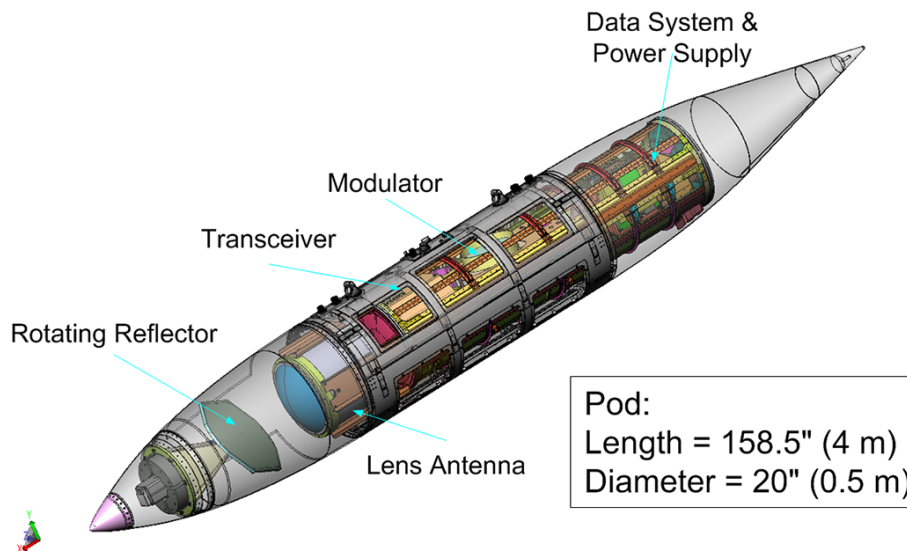


Figure 2. Side view of the 20'' HIAPER wing pod showing the layout of the radar electronics. The front of the pod is on the left hand side of the figure. The reflector plate is positioned such that the beam clears the leading edge of the wing when pointing toward zenith.

A wing pod-based millimeter wavelength airborne cloud radar

J. Vivekanandan et al.

Title Page

Abstract

Introduction

Conclusions

References

Tables

Figures



Back

Close

Full Screen / Esc

Printer-friendly Version

Interactive Discussion



Discussion Paper | Discussion Paper | Discussion Paper | Discussion Paper | Discussion Paper

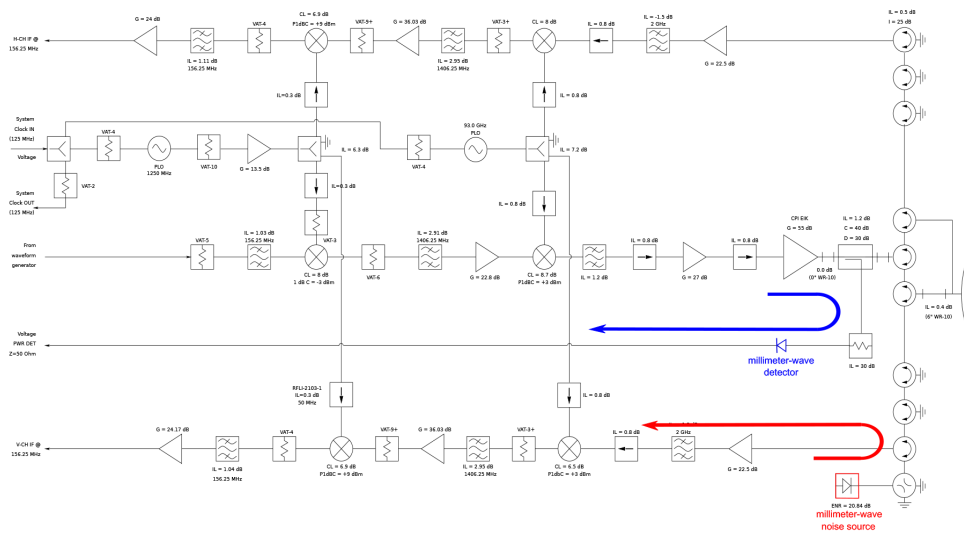


Figure 3. Block diagram of polarimetric HCR transceiver. The blue arrow couples the transmit signal for monitoring the transmitted power. The red arrow shows the signal path for monitoring receiver gain using a known noise source.

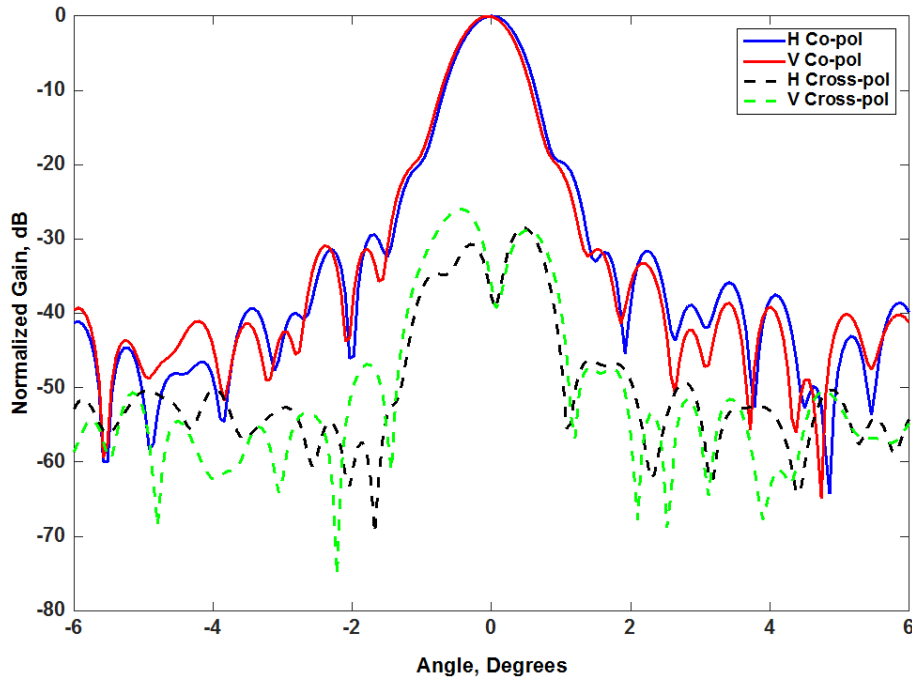


Figure 4. E-Plane co and cross-pol radiation patterns of HCR's lens antenna.

A wing pod-based millimeter wavelength airborne cloud radar

J. Vivekanandan et al.

Title Page	
Abstract	Introduction
Conclusions	References
Tables	Figures
◀	▶
◀	▶
Back	Close
Full Screen / Esc	
Printer-friendly Version	
Interactive Discussion	



A wing pod-based millimeter wavelength airborne cloud radar

J. Vivekanandan et al.

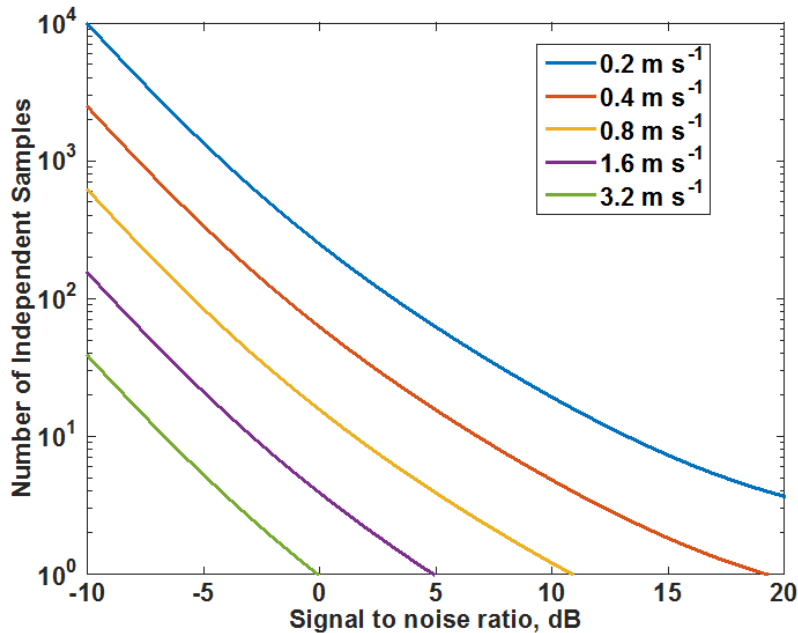


Figure 5. Velocity accuracy as a function of independent samples and signal-to-noise ratio. Spectrum width is assumed 1 ms^{-1} PRF is 10 kHz and transmit frequency is W-band.

[Title Page](#)[Abstract](#)[Introduction](#)[Conclusions](#)[References](#)[Tables](#)[Figures](#)[⏪](#)[⏩](#)[◀](#)[▶](#)[Back](#)[Close](#)[Full Screen / Esc](#)[Printer-friendly Version](#)[Interactive Discussion](#)

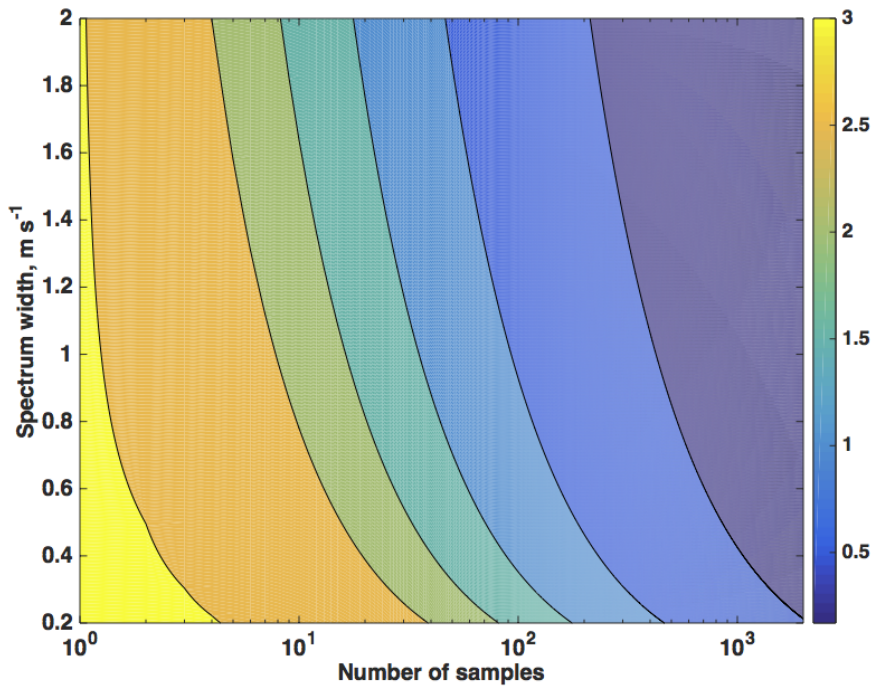


Figure 6. Standard error in reflectivity measurements. For a specified number of samples, standard error in reflectivity becomes lower as the Doppler spectrum becomes broader. For greater than 1000 samples, standard error in reflectivity is < 0.5 dB.

A wing pod-based millimeter wavelength airborne cloud radar

J. Vivekanandan et al.

[Title Page](#)

[Abstract](#) | [Introduction](#)

[Conclusions](#) | [References](#)

[Tables](#) | [Figures](#)

[◀](#) | [▶](#)

[◀](#) | [▶](#)

[Back](#) | [Close](#)

[Full Screen / Esc](#)

[Printer-friendly Version](#)

[Interactive Discussion](#)



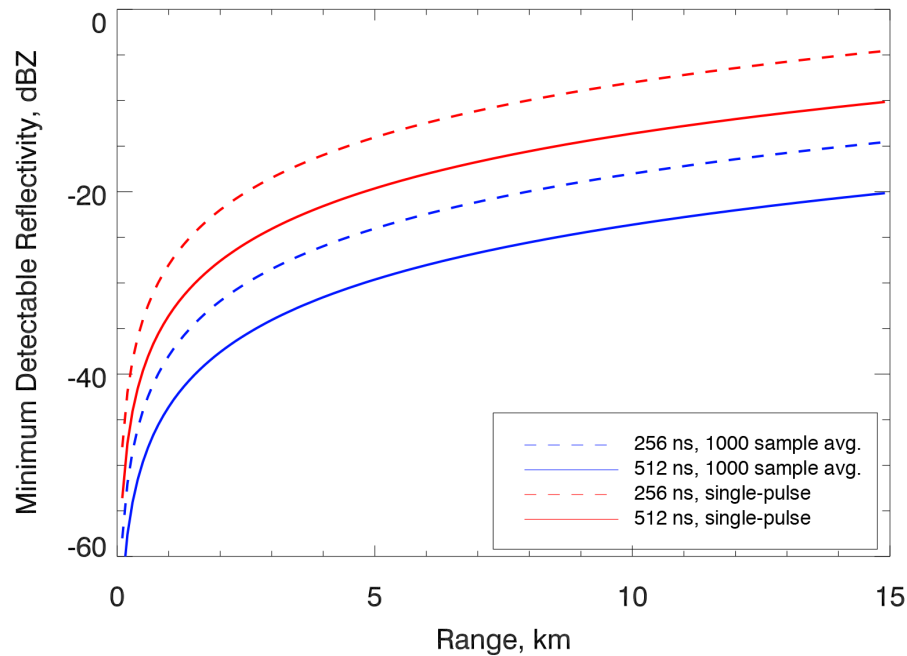


Figure 7. Sensitivity of the HCR as a function of range is shown for two different transmit pulse widths and also for no averaging and averaging over 1000 samples.

A wing pod-based millimeter wavelength airborne cloud radar

J. Vivekanandan et al.

[Title Page](#)

[Abstract](#) | [Introduction](#)

[Conclusions](#) | [References](#)

[Tables](#) | [Figures](#)

[◀](#) | [▶](#)

[◀](#) | [▶](#)

[Back](#) | [Close](#)

[Full Screen / Esc](#)

[Printer-friendly Version](#)

[Interactive Discussion](#)



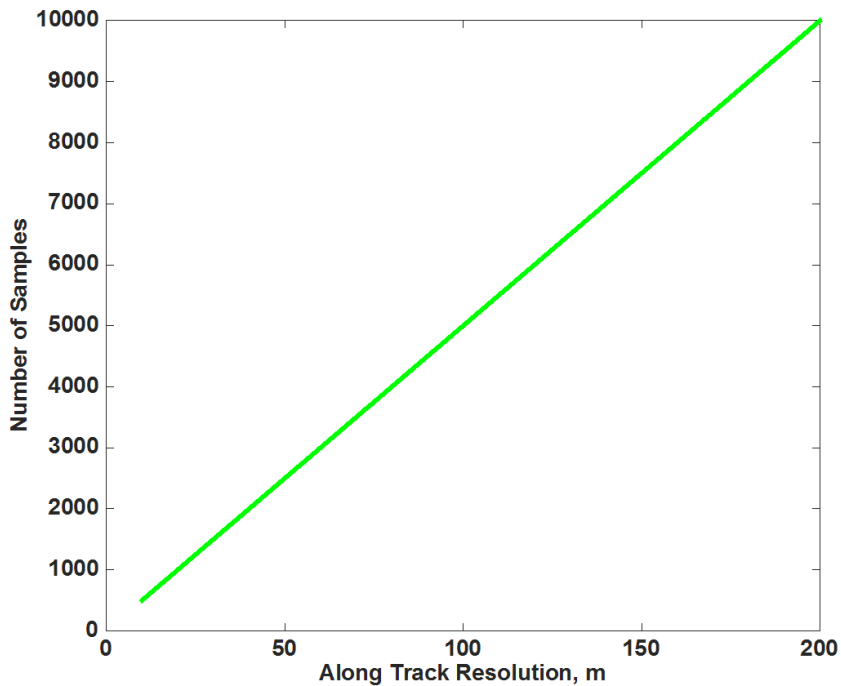


Figure 8. Number of samples verses along track resolution is shown. The PRF is assumed 10 000 Hz. Aircraft speed is assumed to be 200 m s^{-1} .

GID

5, 117–159, 2015

A wing pod-based millimeter wavelength airborne cloud radar

J. Vivekanandan et al.

[Title Page](#)

[Abstract](#) | [Introduction](#)

[Conclusions](#) | [References](#)

[Tables](#) | [Figures](#)

[◀](#) | [▶](#)

[◀](#) | [▶](#)

[Back](#) | [Close](#)

[Full Screen / Esc](#)

[Printer-friendly Version](#)

[Interactive Discussion](#)



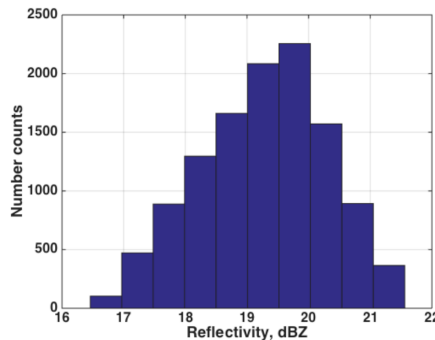
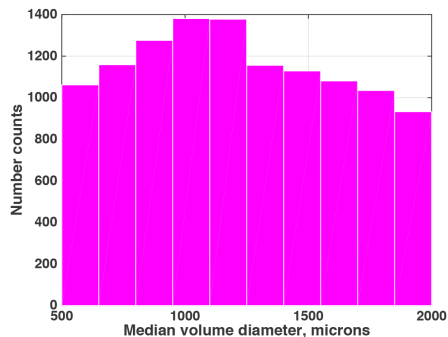
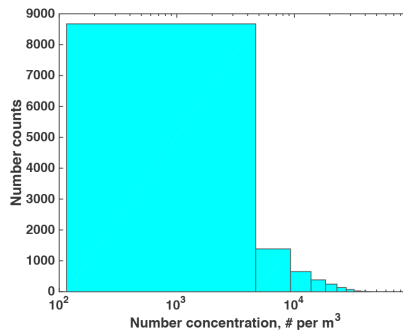
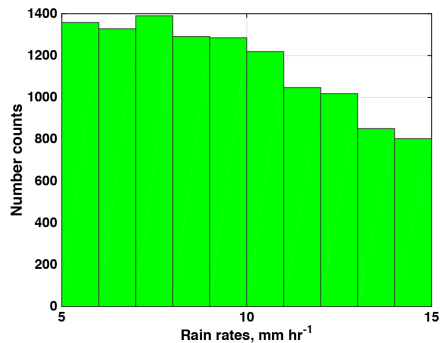


Figure 9. Histograms of rain rates, raindrop size distributions and computed W-band reflectivities: **(a)** rain rate, **(b)** concentration, **(c)** median volume diameter, and **(d)** reflectivity. Mean value of reflectivity is 19 dBZ and SD is less than dB for rain rates between 5 and 15 mm h⁻¹.

A wing pod-based millimeter wavelength airborne cloud radar

J. Vivekanandan et al.

[Title Page](#)

[Abstract](#)

[Introduction](#)

[Conclusions](#)

[References](#)

[Tables](#)

[Figures](#)

[⏪](#)

[⏩](#)

[◀](#)

[▶](#)

[Back](#)

[Close](#)

[Full Screen / Esc](#)

[Printer-friendly Version](#)

[Interactive Discussion](#)



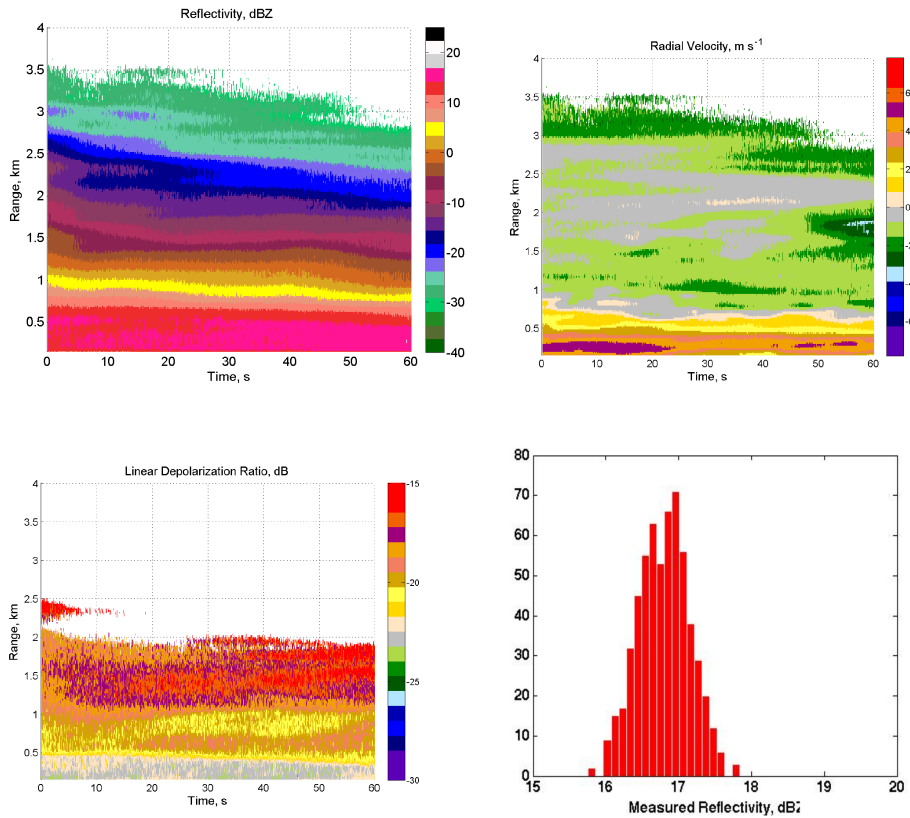


Figure 10. Radar measurements in stratiform rain. The HCR was on the ground and the beam was pointing at 30 elevation. The B-scan display shows time versus range for the following: **(a)** reflectivity, **(b)** velocity and **(c)** LDR. A histogram of reflectivity at 200 m is shown in the last panel.

A wing pod-based millimeter wavelength airborne cloud radar

J. Vivekanandan et al.

Title Page

Abstract

Introduction

Conclusions

References

Tables

Figures

⏪

⏩

◀

▶

Back

Close

Full Screen / Esc

Printer-friendly Version

Interactive Discussion



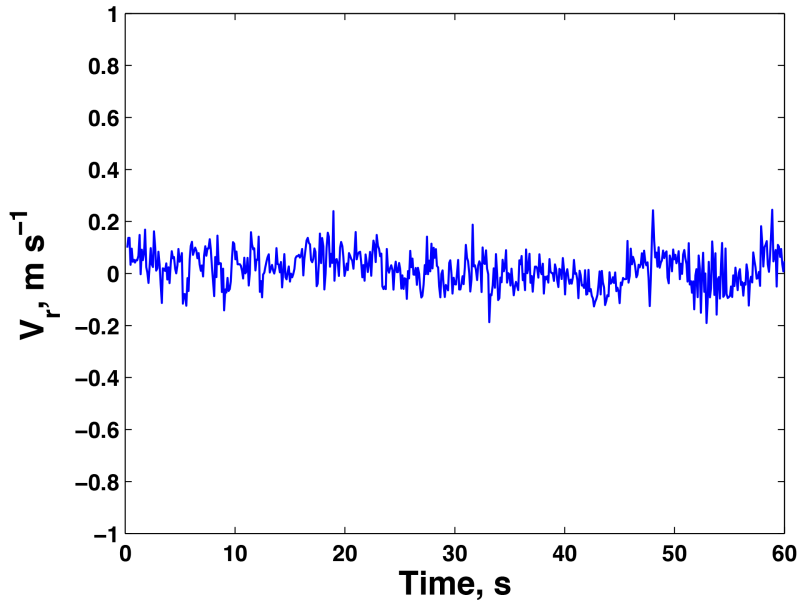


Figure 11. One minute of corrected V_r data within ground echo measured during the test flight of 3 October 2014.

A wing pod-based millimeter wavelength airborne cloud radar

J. Vivekanandan et al.

Title Page

Abstract Introduction

Conclusions References

Tables Figures

◀ ▶

◀ ▶

Back Close

Full Screen / Esc

Printer-friendly Version

Interactive Discussion



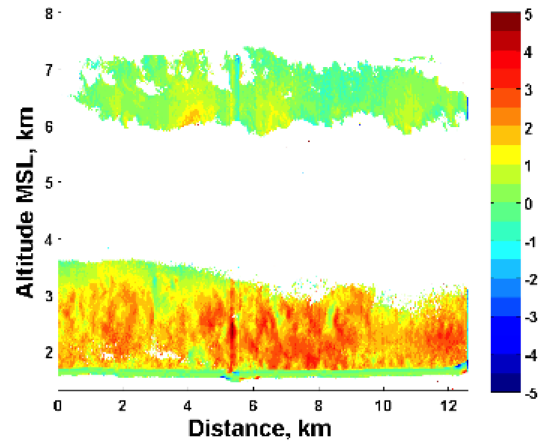
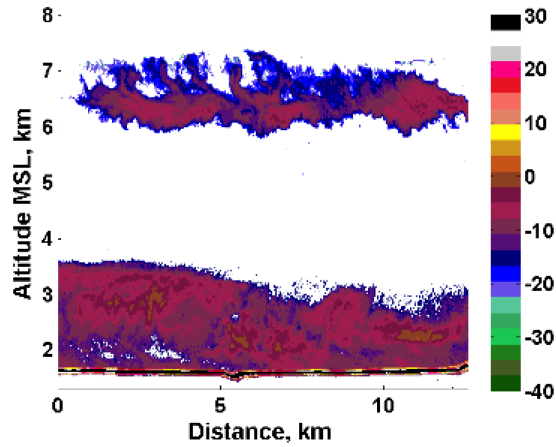


Figure 12. B-scan plots of Z_e and V_r collected 23 February 2013 from the HCR looking nadir.

A wing pod-based millimeter wavelength airborne cloud radar

J. Vivekanandan et al.

[Title Page](#)

[Abstract](#)

[Introduction](#)

[Conclusions](#)

[References](#)

[Tables](#)

[Figures](#)

⏪

⏩

◀

▶

[Back](#)

[Close](#)

[Full Screen / Esc](#)

[Printer-friendly Version](#)

[Interactive Discussion](#)



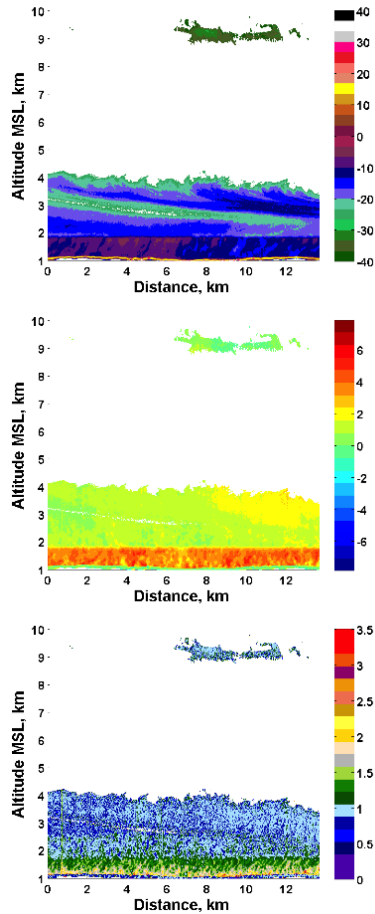


Figure 13. B-scan plots of Z_e , V_r and spectrum width collected on 11 October 2013 from the HCR looking nadir.

A wing pod-based millimeter wavelength airborne cloud radar

J. Vivekanandan et al.

[Title Page](#)

[Abstract](#)

[Introduction](#)

[Conclusions](#)

[References](#)

[Tables](#)

[Figures](#)

⏪

⏩

◀

▶

[Back](#)

[Close](#)

[Full Screen / Esc](#)

[Printer-friendly Version](#)

[Interactive Discussion](#)



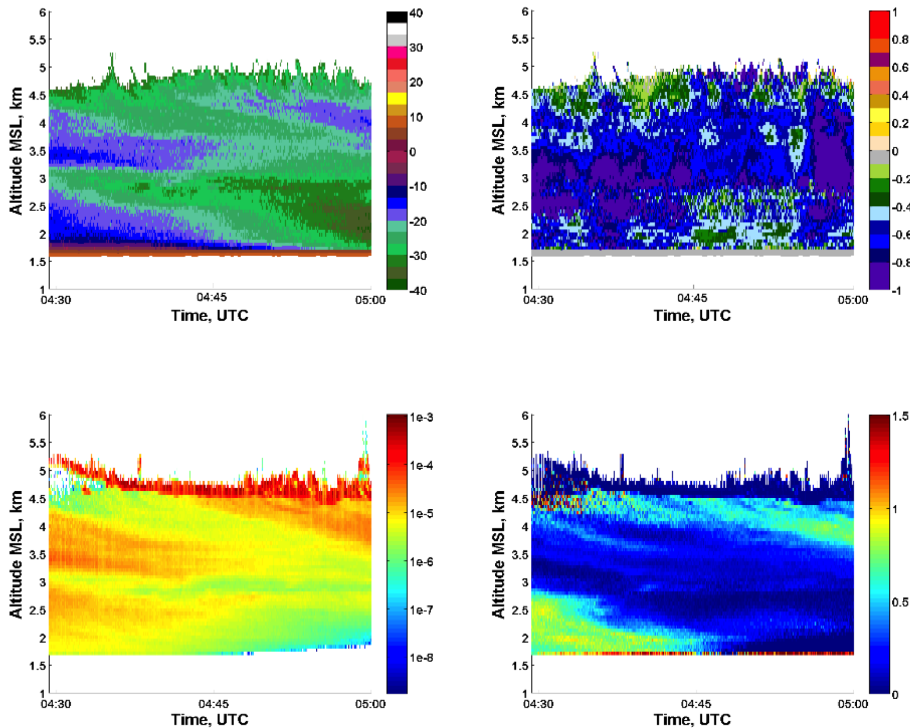


Figure 14. Coincident ground-based HCR and HSRL measurements of liquid and ice clouds. **(a)** W-band reflectivity, **(b)** W-band radial velocity, **(c)** lidar backscatter and **(d)** lidar circular depolarization ratio. Data were collected on 22 November 2013.

A wing pod-based millimeter wavelength airborne cloud radar

J. Vivekanandan et al.

[Title Page](#)

[Abstract](#)

[Introduction](#)

[Conclusions](#)

[References](#)

[Tables](#)

[Figures](#)

[⏪](#)

[⏩](#)

[◀](#)

[▶](#)

[Back](#)

[Close](#)

[Full Screen / Esc](#)

[Printer-friendly Version](#)

[Interactive Discussion](#)



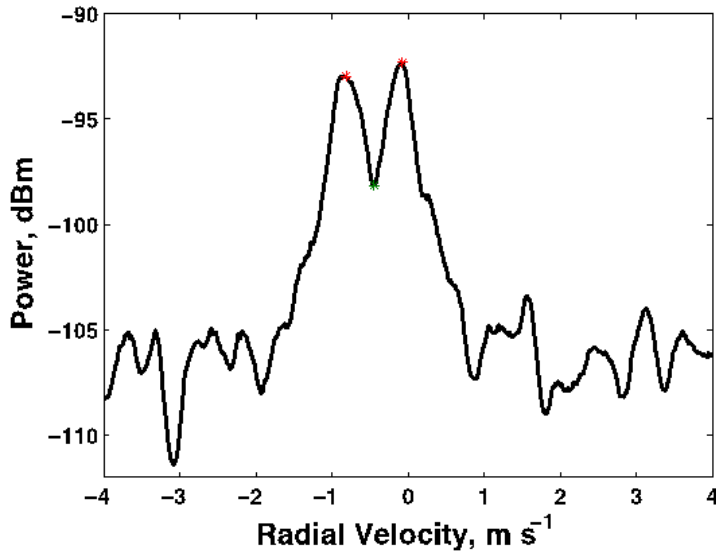


Figure 15. HCR spectrum collected in a mixed phase cloud. The radar was ground-based and pointed vertically.

A wing pod-based millimeter wavelength airborne cloud radar

J. Vivekanandan et al.

Title Page	
Abstract	Introduction
Conclusions	References
Tables	Figures
⏪	⏩
◀	▶
Back	Close
Full Screen / Esc	
Printer-friendly Version	
Interactive Discussion	

